On The Contribution of Local Current Density to Neoclassical Tearing Mode Stabilisation

O. Sauter*

Centre de Recherches en Physique des Plasmas,

Association EURATOM-Confédération Suisse,

EPFL, PPB-Ecublens, 1015 Lausanne, Switzerland

(Dated: July 9, 2004)

Abstract

Neoclassical tearing modes are driven by the reduction of bootstrap current inside the island due to the flattening of the pressure profile. This current perturbation enhances the magnetic perturbation responsible for the island formation. Therefore it is well-known that local current drive (CD) can be used to compensate this perturbation and stabilize the mode. Several forms of the current drive contribution to the modified Rutherford equation have been proposed. Analytical fits of these contributions are provided in order to facilitate their comparison with experiments and a new contribution is proposed. Since the bounce and transit frequencies are much larger than the collision frequency and the modulation frequency of the CD source in phase with the island, it is argued that the effective current driven density profile is a flux function. Assuming an exponential profile leads to no difference between modulated and continuous application of current drive. The various forms differ mainly at small island width and the possibility to differentiate amongst them experimentally is discussed.

*Electronic address: olivier.sauter@epfl.ch

I. INTRODUCTION

Tearing modes in tokamak plasmas have been studied for many years and the possibility to "compensate" the perturbed parallel current within the island in order to stabilise them has been proposed more than twenty years ago [1]. It has also been seen that local heating can stabilise the mode by modifying the local resistivity and hence the local inductive current [2]. However this latter effect is usually smaller than the current drive (CD) contribution and therefore is not discussed in this paper.

The contribution to the modified Rutherford equation [3], which governs the nonlinear time evolution of the island width with respect to the perturbed parallel electric field in the vicinity of the island, has been calculated by several authors [4]-[9]. This has become more important due to the presence of neoclassical tearing modes (NTM) in long pulse ELMy H-mode scenarios (high confinement scenario with edge localised modes), which can degrade the energy and particle confinement even at low β [10]. These modes are tearing modes with a sufficiently large island width, typically larger than $2-3cm$, such that the perturbed bootstrap current drives the island to a much larger saturated island width, up to typically $10-20cm$ in present tokamaks ($10-20\%$ of the minor radius). With such saturated widths, a confinement degradation exceeding 20% is predicted for the standard scenario in the international thermonuclear experimental reactor (ITER-FEAT) [11], which is unacceptable in order to fullfill the main goals of this experiment. Therefore it is proposed to use electron cyclotron current drive (ECCD) to stabilise or reduce significantly the size of the NTM. This has been achieved successfully in several tokamaks [12]-[14], however the predictions of the requirements for the ECCD system are still in question and this is the principal application of this paper.

II. CD CONTRIBUTION TO THE MODIFIED RUTHERFORD EQUATION

The modified Rutherford equation, for the island evolution of a m/n tearing mode (with m the poloidal and n the toroidal mode numbers) can be written as follows, using the notation of Ref. [15]:

$$\frac{dw}{dt} = \frac{\rho_s}{\tau_{\mathrm{R}}} \left[\rho_s \Delta' + \rho_s \Delta'_{bs} + \rho_s \Delta'_{GGJ} + \rho_s \Delta'_{pol} + \rho_s \Delta'_{cd} + \rho_s \Delta'_{H} \right], \tag{1}$$

The first term on the right-hand side is the classical Δ' term determined by the total equilibrium current density profile, the second term relates to the perturbed bootstrap current and is the driving term. The GGJ term is due to the stabilising effect of curvature [16], the next is due to the polarisation current and is usually assumed stabilising [17]. The last term of Eq. (1) relates to the modification of the local conductivity within the island by localised heating [5]. Since it is usually smaller than the CD term, we shall not discuss it here. The term $\rho_s\Delta'_{cd}$ is the current drive contribution we shall discuss in this paper, in relation to the bootstrap term $\rho_s\Delta'_{bs}$. The bootstrap contribution can be written as:

$$\rho_s\Delta'_{bs} = \rho_s\beta_p\frac{a_{bs}\ w}{w^2+w_d^2}, \tag{2}$$

where a_{bs} depends essentially on the q and pressure scalelengths as well as on geometrical factors. Equation (1) is obtained through adequate averaging of Ohm's law over helical flux surfaces in the vicinity of the island. Following the detailed description in Ref. [18], we can write (Eq. (103) of Ref. [18]):

$$\frac{\delta\Psi}{\delta t}\ \cos\alpha = -\ \eta(\rho_s)(\delta j_{\|} - \delta j_{bs} - \delta j_{cd}) - \mathbf{b}\cdot\nabla\mathbf{\Phi}, \tag{3}$$

where α is the helical phase ($=\theta-\frac{n}{m}(\phi-\omega t)$), Ψ the perturbed poloidal flux near the island, η the resistivity, and $\delta j_{\|}, \delta j_{bs}, \delta j_{cd}$ are the total, bootstrap and non-inductive perturbed current density. In this paper, we neglect the modification of the equilibrium current profile with CD, which can modify the Δ' contribution [19],[20]. It is convenient to define the helical flux:

$$\chi = -\int_{\rho_s}^{\rho}(1-\frac{q}{q_s})B_\theta \mathrm{d}\rho - \Psi(\rho)cos(m\alpha), \tag{4}$$

since $(\mathbf{B}+\delta\mathbf{B})\cdot\nabla\mathbf{B}=\mathbf{0}$ and χ maps out the perturbed magnetic flux surfaces. Let us then define the helical flux surface average using a similar notation as in Ref. [7]: $\psi(=(\chi-\Psi)/2\Psi)$ is the helical flux surface label with $\psi=-1$ at the O-point of the island and $\psi=0$ at the X-point (however keeping w as the full island width):

$$< A >= \frac{1}{2\pi}\int_0^{2\pi}\mathrm{d}\alpha\frac{A}{\sqrt{\psi+\cos^2(\frac{m\alpha}{2})}}. \tag{5}$$

In this way the CD term is given by:

$$\rho_s\Delta'_{cd} = -\ \frac{16\ \mu_0\ \rho_s\ L_q}{B_p\ w}\int_{-1}^{\infty}\mathrm{d}\psi\ \frac{< j_{cd} >}{< 1 >}\ < \cos\ m\alpha >. \tag{6}$$

To evaluate further the CD contribution, one has to define the current drive profile j_{cd} in terms of ψ and α. Its normalisation is given by the total driven current I_{cd}. If j_{cd} is known in real space (ρ, θ) or in terms of (ψ, α), one can normalise it as such, using $j_{cd} = j_{cd0}\ \tilde{j}_{cd}(\psi, \alpha)$:

$$I_{cd} = \int \rho\ \mathrm{d}\rho\ \mathrm{d}\theta\ j_{cd}(\rho, \theta) = \frac{j_{cd0}\ \rho_s\ w}{2} \int_{-1}^{\infty} \mathrm{d}\psi \int \mathrm{d}\alpha \frac{\tilde{j}_{cd}(\psi, \alpha)}{\sqrt{\psi + \cos^2(\frac{m\alpha}{2})}}, \tag{7}$$

with $\tilde{j}_{cd}(\rho - \rho_s, \theta) \rightarrow \tilde{j}_{cd}(\frac{w}{2}\sqrt{\psi + \cos^2(\frac{m\alpha}{2})}, \alpha)$ and j_{cd0} used to single out the normalisation. Therefore the term j_{cd} in Eq. (6) can be evaluated substituting j_{cd0} by I_{cd} using Eq. (7), yielding:

$$\rho_s \Delta'_{cd} \ = \ - \frac{16\ \mu_0\ L_q\ I_{cd}}{\pi\ B_p\ w_{cd}^2}\ \tilde{\eta}_{aux}(\frac{w}{w_{cd}}), \tag{8}$$

with

$$\tilde{\eta}_{aux}(w/w_{cd}) = \frac{w_{cd}^2}{w^2}\ \frac{\int_{-1}^{\infty} \mathrm{d}\psi\ J(\psi)\ W(\psi)}{\int_{-1}^{\infty} \mathrm{d}\psi\ J(\psi)\ V(\psi)}, \tag{9}$$

and where we have used the functions defined in Ref. [7]:

$$J(\psi) \ = \ \frac{1}{V(\psi)}\ \int \mathrm{d}\alpha \frac{\tilde{j}_{cd}(\psi, \alpha)}{\sqrt{\psi + \cos^2(\frac{m\alpha}{2})}}, \tag{10}$$

$$W(\psi) \ = \ \int \mathrm{d}\alpha \frac{\cos(m\alpha)}{\sqrt{\psi + \cos^2(\frac{m\alpha}{2})}}, \tag{11}$$

$$V(\psi) \ = \ \int \mathrm{d}\alpha \frac{1}{\sqrt{\psi + \cos^2(\frac{m\alpha}{2})}}. \tag{12}$$

Note that these quantities are directly related to the terms in Eq.(6):

$$J(\psi) \ = \ \frac{2\ \pi}{V(\psi)}\ < \tilde{j}_{cd} >, \tag{13}$$

$$W(\psi) \ = \ 2\pi\ < \cos(m\alpha) >, \tag{14}$$

$$V(\psi) \ = \ 2\pi\ < 1 > . \tag{15}$$

The part which is under discussion in this paper is the term $\tilde{\eta}_{aux}(w/w_{cd})$ defined in Eq. (9), which contains all the terms depending on the island width w. If $\tilde{j}_{cd}(\psi, \alpha) = \tilde{j}_{cd}(\psi)$ is a flux function, as assumed in [5], then $\tilde{\eta}_{aux}$ reduces to:

$$\tilde{\eta}_{aux}(w/w_{cd}) = \frac{w_{cd}^2}{w^2}\ \frac{\int_{-1}^{\infty} \mathrm{d}\psi\ W(\psi)\ \tilde{j}_{cd}(\psi)}{\int_{-1}^{\infty} \mathrm{d}\psi\ V(\psi)\ \tilde{j}_{cd}(\psi)}. \tag{16}$$

The total current, $\delta j_{\|}$ in Eq.(3), has been assumed to be a flux function in order to evaluate the classical Δ' term in Eq. (1). In addition, the bounce and transit frequencies are much larger than the collision frequency, as well as of the modulation frequency, of a few kHz, proposed to drive current in the O-point of the island. For example the current profile outside the island is calculated using bounce-averaged Fokker-Planck equations and ray-tracing codes which typically give a flux surface current density profile of the form:

$$j_{cd}(\rho) = j_{cd0}\ \exp\Big[-\frac{4(\rho-\rho_{cd})^2}{w_{cd}^2}\Big], \tag{17}$$

where ρ_{cd} is the deposition location and w_{cd} the full e^{-1} current density width. Note that in the torus, $j_{cd} = f(\psi)B$, the poloidal variation of j_{cd} follows the magnitude of B. Therefore assuming that j_{cd} is a flux function is in fact assuming that $< \mathbf{j_{cd}} \cdot \mathbf{B} > / < \mathbf{B^2} >$ is equal to $j_{cd}/B = f(\psi)$, where $< . >$ are flux surface averages. The main point here is that $f(psi)$ applies even if the wave-particle interaction happens in a poloidally localised region of the plasma. Following similar arguments, we can expect the current profile within the island to also be a helical flux function and therefore Eq. (16) to apply.

In Ref. [5], $\tilde{j}_{cd}(\psi)$ was chosen as a box-type function given by a Heavyside function:

$$\tilde{j}_{cd}(\psi) = \tilde{j}_{cd0}\ H(\psi_0 - \psi), \tag{18}$$

with $\psi_0 = \psi_{box} = w_{cd}^2/w^2 - 1$. This corresponds to the ψ_1 flux surface shown in Fig.1 (solid circle). Since $x = \pm\frac{w}{2}\sqrt{\psi + \cos^2(\frac{m\alpha}{2})}$, Eq.(18) corresponds to a current driven inside the flux surface at $x = \frac{w_{cd}}{2}, \alpha = 0$. Thus it simulates a modulation such that the current is driven at the O-point, inside $\psi_1 = \psi_{box}$, with a small on-time corresponding to the box with a small extension in the helical direction α as shown in Fig. 1 (solid line rectangle). Note that if the modulation of the ECCD source is such that it is 50% on-50% off, centered at the O-point, it would drive current in the dashed box marked on Fig. 1. Assuming a helical flux function, the modulated ECCD source would effectively drive a non-zero current inside $\psi = \psi_2$, with $\psi_2 = \psi_{box} + 1/2$. In the case of no modulation, one sees that the current drive density extends to the surface $\psi_3 = \psi_{box} + 1$, which is actually outside the island. In this example, one immediatly sees that if $\psi_{box} >> 1$, the difference between $\psi_{box}, \psi_{box} + 1/2$ and $\psi_{box} + 1$ is negligible. In other words, when $w/w_{cd} < 0.5$, there is no difference between modulation and continuous waveform (CW) in $\tilde{\eta}_{aux}$, contrary to what is found if one allows for non-flux surface current deposition as in Refs. [4], [6]-[9], as will be discussed below. In

addition, as I_{cd} is larger at constant power for the CW case, it would be more efficient to keep CW-ECCD.

The box-type current deposition profile described above was used in order to obtain an analytical form for $\tilde{\eta}_{aux}(w)$ [5]. However a more realistic deposition profile is the form given in Eq. (17), which yields as a function of ψ:

$$\tilde{j}_{cd}(\psi) = \tilde{j}_{cd0} \;\; exp\Big[-\frac{w^2}{w_{cd}^2}\;\Big(\psi + \cos^2(\frac{m\alpha_0}{2})\Big)\Big], \tag{19}$$

where $m\alpha_0$ corresponds to the maximum angle reached during the on-time. For example, if the on-time is small, the current is driven only around the O-point as in the small box case and $m\alpha_0 \approx 0$. Note that replacing ψ by $\psi_1 = w_{cd}^2/w^2 - 1$, one finds $\tilde{j}_{cd}(\psi_1) = \tilde{j}_{cd0}\; e^{-1}$. Thus we have replaced the box-type profile with a Gaussian profile of similar characteristic width. The case of 50% on-time, with $m\alpha_0 = \pi/2$, corresponds to a Gaussian with e^{-1} width at $\psi = \psi_2$ and the CW case is obtained with $m\alpha_0 = \pi$ and e^{-1} at $\psi = \psi_3$. An important consequence of the function given in Eq. (19) is that the phase factor related to the fraction of source modulation is independent of ψ. Therefore, once included in Eq. (16), the numerator and denominator terms cancel exactly and $\tilde{\eta}_{aux}(w)$ is independent of the modulation frequency.

The numerical calculations of $\tilde{\eta}_{aux}(w)$, Eq. (16), using $\tilde{j}_{cd}$ given by Eq. (18) with $\psi_0 = \psi_1$, ψ_2 or ψ_3, and using Eq. (19), are shown in Fig. 2 as a function of w/w_{cd}. The analytical result of Ref. [5], Eq.(17), is also shown (dashed line) to check our numerical integration. It compares well with the numerical result (solid line). As mentioned above, the box-type results are similar when $w/w_{cd} < 0.5$. Note that $w/w_{cd} \approx 0.5$ is actually the expected value at full stabilisation in ITER-FEAT [11], assuming a characteristic deposition width of $10cm$ and a marginal island width of the order of $5cm$. The result of the flux surface (fs) Gaussian profile (solid line with circles), using Eq. (19), can be fitted with:

$$\tilde{\eta}_{auxfs}(w) = \frac{6}{(w/w_{cd})^4 + 40} \;+\; \frac{1}{(w/w_{cd})^2 \;+\; 10} \tag{20}$$

If one does not assume flux surface functions for the current drive term, then Eq.(9) has to be used with, for example, as proposed in Refs. [4], [6]-[9]:

$$\tilde{j}_{cd}(\psi, \alpha) = M(\alpha)\; exp\Big[-\frac{w^2}{w_{cd}^2}\;\Big(\psi + \cos^2(\frac{m\alpha}{2})\Big)\Big], \tag{21}$$

where $M(\alpha)$ is one for the helical extension α where the ECCD is turned on and zero otherwise. Introducing Eq. (21) into Eq. (9), we obtain the results shown in Fig. 3 (50%-

on solid, CW dashed). The function proposed in Ref. [21], $f(w)/(w^2/w_{cd}^2)$ is also shown (dashed-dotted). A better and simpler fit of the 50% on-case can be obtained with:

$$\tilde{\eta}_{auxloc}(w, 50\%) = 0.9\ \tanh(\frac{w}{2.5w_{cd}})\ \frac{w_{cd}^2}{w^2}. \tag{22}$$

The CW case, assuming local current deposition, can be fitted with [22]:

$$\tilde{\eta}_{auxlocCW}(w) = \frac{0.25}{1\ +\ \frac{2}{3}(\frac{w}{w_{cd}})^2}. \tag{23}$$

To really compare the different contributions, one has to add a factor related to the effective total current driven in the case of modulation (0.5 for the 50% on-time case). This is shown in Fig. 4 for the "fs" Gaussian profiles corresponding to $\tilde{\eta}_{auxfs}$ of Eq. (20) (solid line), to $0.5\tilde{\eta}_{auxloc}(w, 50\%)$ of Eq. (22) (dashed line), and to $\tilde{\eta}_{auxlocCW}$ of Eq. (23) (dashed-dotted line). The dotted lines correspond to the respective fits referred to in these equations. It is seen that the modulated case, assuming local current deposition, differs significantly from the similar CW case only for $w < w_{cd}$. In addition it is significantly larger than the flux-surface Gaussian-type profile only for $w/w_{cd} < 0.5$. The function used in Ref. [13] is also shown (dotted line), without the factor 0.4, as it turns out to be very close to the present proposed form, the latter being independent of modulation frequency.

III. FLUX SURFACE VS α-DEPENDENT CURRENT DRIVE PROFILE

Let us discuss in more detail the difference between the assumption proposed in this paper, namely that the current density profile can be a helical ψ flux surface function, of approximately Gaussian type in ρ, and a local current density which varies strongly along the helical angle α, as given by the function $M(\alpha, \tau)$ used in Eq. (21). The latter could lead to a sharp poloidal variation of $E_\parallel$, with different responses from electrons and ions, and to the break-down of the quasi-neutrality condition. Thus a kinetic treatment is required, taking into account the finite ion Larmor radius and banana widths. This is out of the scope of this paper, but to be able to compare the two assumptions, we can construct the equivalent flux surface current density contributing to the Δ'_{cd} term. It is given by:

$$\bar{j}(\psi)\ =\ \frac{J(\psi)}{\int \mathrm{d}\psi JV}, \tag{24}$$

where $J(\psi)$ is given in Eq.(10). Note that if $\tilde{j}_{cd}(\psi, \alpha) = \tilde{j}_{cd}(\psi)$ is a flux function, then $J(\psi) = \tilde{j}_{cd}(\psi)$.

In Fig. 5, we show three different forms of $M(\alpha)$, (A, B and C) used to calculate the current contribution, based on $(0.5 - 0.5\ \tanh((m\alpha - \alpha_\tau)/0.06))$, with $\alpha_\tau = \pi/2, 3\pi/4$ and π. This function is used to avoid any discontinuities in $M(\alpha)$. Note that modifying the rate of change (0.06 above), which can mimic the effective turn on and off of the gyrotrons, does not change significantly the results as shown below. In Fig. (6a), we show the resulting $\bar{j}(\psi)$ profiles for the three cases A, B and C, factorising in the effective current driven (I_{cd}/I_{CW}, e.g. 0.5 for A), as well as the fs profile, using Eq. (19), for comparison. Also shown in Fig. (6b) is $W(\psi)$ which represents the weight of the contribution of the local current density to the Δ'_{cd} term ($\sim \int \bar{j} W$). It is positive, stabilising, near the O-point, and very negative in a small region near the X-point. This explains why any finite contribution of J near $m\alpha = \pi$ is destabilising. Fig. (6a) shows that if $\tilde{\bar{j}}_{cd}(\psi, \pi) = 0$, there is a strong dip in $\bar{j}$ near $\psi = 0$, which allows for the $1/w$ dependence of Δ'_{cd} as shown in Fig. 7. When non-zero current is driven near $m\alpha = \pi$, the contribution at, for example, $w/w_{cd} = 0.5$ decreases rapidly, until the $1/w$ dependence is lost as in the CW case. To illustrate this point we have calculated η_{aux} with $M(\alpha) = 0.75 - 0.25\ tanh((m\alpha - 3\pi/4)/\delta\alpha)$, with $\delta\alpha = 0.06$ and 0.4 (dotted lines, D, in Fig. 5). These give exactly the same result for η_{aux}, as shown in Fig. 7 (circles), and lead to similar contributions at $w/w_{cd} = 0.5$ as the fs flux-surface case, $\eta_{aux} \approx 0.26$. Note also that for the case C, $\alpha_\tau = \pi$ of Fig. 5, $\bar{j}(\psi)$ is actually larger than the flux-surface case fs near the X-point. This is why the resulting Δ'_{cd} term is smaller in the CW local case than assuming a flux surface function. Therefore the main question is if the "dip" in $\bar{j}(\psi)$ near $\psi = 0$ remains once 5D kinetic effects are taken into account self-consistently, including the possible radial diffusion of fast particles as seen in the Tokamak à configuration variable (TCV) [23], and in particular when the bounce frequency is non-negligible with respect to the modulation frequency. This is actually a complex question since the dip width is smaller than the ion banana width. Recently, this has been modeled using fluid theory and including parallel/perpendicular diffusion of the electrons [24]. This can lead to similar effective current density profiles as shown in Fig. (6a), depending on parallel and perpendicular diffusion coefficients and on the slowing down time. This can explain the decrease in stabilising efficiency when $\chi_\perp$ increases or when the slowing down time increases.

From Eqs. (1) and (9), a simple figure of merit for the CD term is given by I_{cd}/w_{cd}^2. Since the CD term needs essentially to compensate for the Bootstrap drive at the maximum

growth rate, which is usually obtained at $w \approx w_{marg}$ [15], we can use the condition:

$$-\Delta'_{cd} - \Delta' \geq -\Delta'_{cd} \;\geq\; \Delta'_{bs}, \tag{25}$$

to define the pessimistic figure of merit. However, since without ECCD we have $-\Delta' \sim \Delta'_{bs}$ at marginal state, one cannot neglect the stabilising contribution from Δ'. Using $f_{\Delta'} = -\Delta'/\Delta'_{bs}$, we can rewrite:

$$-\Delta'_{cd} \;\geq\; (1 \;-\; f_{\Delta'})\; \Delta'_{bs}. \tag{26}$$

With $\rho_s \Delta'_{bs} = \rho_s \beta_p a_{bs}/2w_{marg}$ and $j_{bs} = (p/B_p)(L_{bs}/L_p)$ [15], we obtain:

$$F_{cd} = \frac{j_{cd}}{j_{bs}} \frac{w_{marg}}{w_{cd}} \tilde{\eta}_{aux} \;\geq\; 0.1\,(1 \;-\; f_{\Delta'}). \tag{27}$$

For the flux surface current assumption case, $\tilde{\eta}_{aux} \approx 0.25$ is constant for $w \leq w_{cd}$ and we have:

$$F^{fs}_{cd} = \frac{j_{cd}}{j_{bs}} \frac{w_{marg}}{w_{cd}} \;\geq\; 0.4\,(1 \;-\; f_{\Delta'}). \tag{28}$$

One sees that for the flux surface case it is also j_{cd}/w_{cd} which needs to be optimised, as in the calculation using the effect on the "outer layer" [20], which also assumed flux surface non-inductive current by construction. For ITER, we expect $w_{marg}/w_{cd} \approx 0.5$, thus we obtain:

$$\frac{j_{cd}}{j_{bs}} \;\geq\; 0.8\,(1 \;-\; f_{\Delta'}). \tag{29}$$

$f_{\Delta'}$ is actually related to the hysteresis parameter and is expected to be around 1/3-1/2 in ITER, for $\beta_N \approx 1.8$, which means $\mathbf{j_{cd}/j_{bs} \geq 0.4}$ for the optimistic requirement. If $w_{marg} < w_{cd}$ and modulation is able to lead to the $1/w$ dependence of $\tilde{\eta}_{aux}$, we have $0.5\tilde{\eta}_{auxloc} \approx 0.18/(w_{marg}/w_{cd})$ and then the figure of merit reduces to:

$$F^{loc,50\%}_{cd} = \frac{j_{cd}}{j_{bs}} \;\geq\; 0.55\,(1 \;-\; f_{\Delta'}), \tag{30}$$

which is 30% better and where we have included the reduction of I_{cd} due to the 50% on-time. This shows that modulation is advantageous only in the case $w_{marg} < 0.5\; w_{cd}$ and if the current density can have such a poloidal dependence as in Eq. (21). Since it is difficult to measure the effective contribution in experiments, at least a factor of 2 difference is required in order to be able to distinguish between these two figure of merits (requiring $w_{marg} < 0.35\; w_{cd}$). In ITER we should reach values of $w_{marg}/w_{cd} \leq 0.5$. It therefore follows that experiments with and without modulation with $w_{marg}/w_{cd} < 0.5$ are required.

IV. CONCLUSION

In Conclusion, it has been shown that if flux surface current deposition profiles are assumed, consistent with the usual assumption for Δ' calculations and for the bounce-averaged Fokker-Planck equations, no difference between modulated and CW CD cases is expected with respect to the w-dependence. However the effective total driven current, at same installed power, favours the CW option. It is important to note that, once the bounce-average calculations are projected on the helical flux surface coordinate, the deposition profiles are not likely to be exactly of Gaussian form. However this should not lead to significant differences as shown in the comparison with the box-type profiles. Moreover, the effective flux surface profile, assuming an α-dependent deposition, is singular near the X-point, i.e. it is negligible in a small region near the X-point. It is possible that other physical mechanisms will "fill" this dip of current near the X-point, like anomalous fast particle diffusion, and strongly reduce the benefit of local modulation.

Finally it has been shown that experimental results with $w_{marg}/w_{cd} < 0.5$ are required in order to be able to discriminate between the 50% on-time local deposition assumption used in Refs.[4], [6]-[9] and the present flux-surface exponential profile yielding $\tilde{\eta}_{auxfs}$ given in Eq. (20). Consequently, specific experiments have to be designed to first measure w_{marg} and then to broaden the current driven profile such that $w_{cd} > 2\, w_{marg}$.

Acknowledgments

The author is grateful for the useful discussions with Profs H. Zohm, S. Günter and C. Hegna, and with Drs. G. Giruzzi and G. Ramponi. This work was supported in part by the Swiss National Science Foundation.

---

[1] V. Chan, G. Guest, Nucl. Fus. **22**, 272 (1982).

[2] E. Westerhof, Nucl. Fus. **27**, 1929 (1987).

[3] P. H. Rutherford, Phys. Fluids **16**, 1903 (1973).

[4] A. W. Morris, R. Fitzpatrick, T. C. Hender and M. R. O'Brien, in Proceedings of the 19th European Conference on Contr. Fusion and Plasma Phys., Innsbruck, 1992, (European Physical

Society, Petit Lancy, 1992) Europhys. Conf. Abstr. **16C**, I-423.

[5] C.C. Hegna, J.D. Callen, Phys. Plasmas **4**, 2940 (1997).

[6] H. Zohm, Phys. Plasmas bf 4, 4333 (1997).

[7] F. W. Perkins, R. W. Harvey, M. Makowski and M. N. Rosenbluth, in Proceedings of the 24th European Conference on Contr. Fusion and Plasma Phys., Berchtesgaden, 1997, (European Physical Society, Petit Lancy, 1997), Europhys. Conf. Abstr. **21A**, 1017.

[8] G. Giruzzi, M. Zabiego, T.A. Gianakon, X. Garbet, A. Cardinali and S. Bernabei, Nucl. Fusion **39**, 107 (1999).

[9] G. Ramponi, E. Lazzaro, S. Nowak, Phys. Plasmas **6**, 3561 (1999).

[10] O. Sauter, R. J. La Haye, Z. Chang *et al*, Phys. Plasmas **4** , 1654 (1997) and references therein.

[11] R. Aymar, V. A. Chuyanov, M. Huguet, Y. Shimomura, Nuclear Fus. **41**, 1301 (2001).

[12] G. Gantenbein, H. Zohm, G. Giruzzi, S. Günter, F. Leuterer, M. Maraschek, J. Meskat, Q. Yu, Phys. Rev. Lett. **85**, 1242 (2000).

[13] R. J. La Haye, S. Günter, D. A. Humphreys, J. Lohr, T. C. Luce, M. Maraschek, C. C. Petty, R. Prater, J. T. Scoville and E. J. Strait, Phys. Plasmas **9**, 2051 (2002).

[14] A. Isayama, Y. Kamada, S. Ide, K. Hamamatsu, T. Oikawa, T. Suzuki, Y. Neyatani, T. Ozeki, Y. Ikeda, K. Kajiwara, Plasma Phys. Contr. Fusion **42**, L37 (2000).

[15] O. Sauter, R.J. Buttery, R. Felton *et al*, Plasma Phys. Control. Fusion **44**, 1999 (2002).

[16] H. Lütjens, J.-F. Luciani and X. Garbet, Phys. Plasmas **8**, 4267 (2001).

[17] A. B. Mikhailovskii, Contrib. Plasma Phys. **43**, 125 (2003).

[18] R. Fitzpatrick, Phys. Plasmas **2**, 825 (1995).

[19] E. Westerhof, Nucl. Fus. **30**, 1143 (1990).

[20] A. Pletzer, F. W. Perkins, Phys. Plasmas **6**, 1589 (1999).

[21] H. Zohm, G. Gantenbein, A. Gude, S. Günter, F. Leuterer, M. Maraschek, J. Meskat, W. Suttrop, Q. Yu, Phys. Plasmas **8**, 2009 (2001).

[22] F. W. Perkins, R. W. Harvey, 45th APS Conference, Albuquerque, Bull. Am. Phys. Soc. **48** QP1-025 (2003).

[23] P. Nikkola, O. Sauter, R. Behn, S. Coda, I. Condrea, T. P. Goodman, M. H. Henderson, R, W, Harvey, Nuclear Fus.**43**, 1343 (2003).

[24] Q. Yu, X. D. Zhang and S. Günter, Phys. Plasmas **11**, 1960 (2004).

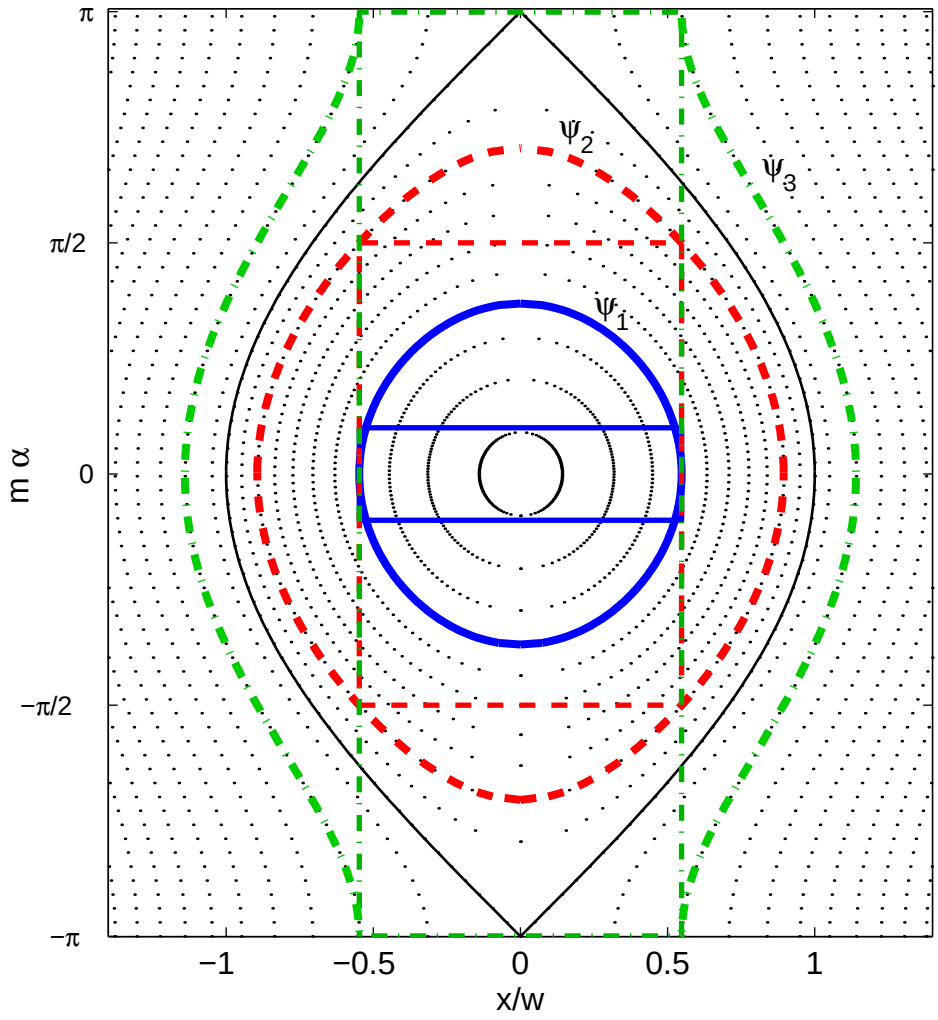

FIG. 1: Island helical flux surfaces ψ and the limiting ψ surfaces related to the box current profiles, spanned with a deposition $w/w_{cd} < 1$ assuming short on-time (ψ_1), 50% on-time (ψ_2) and CW (ψ_3).

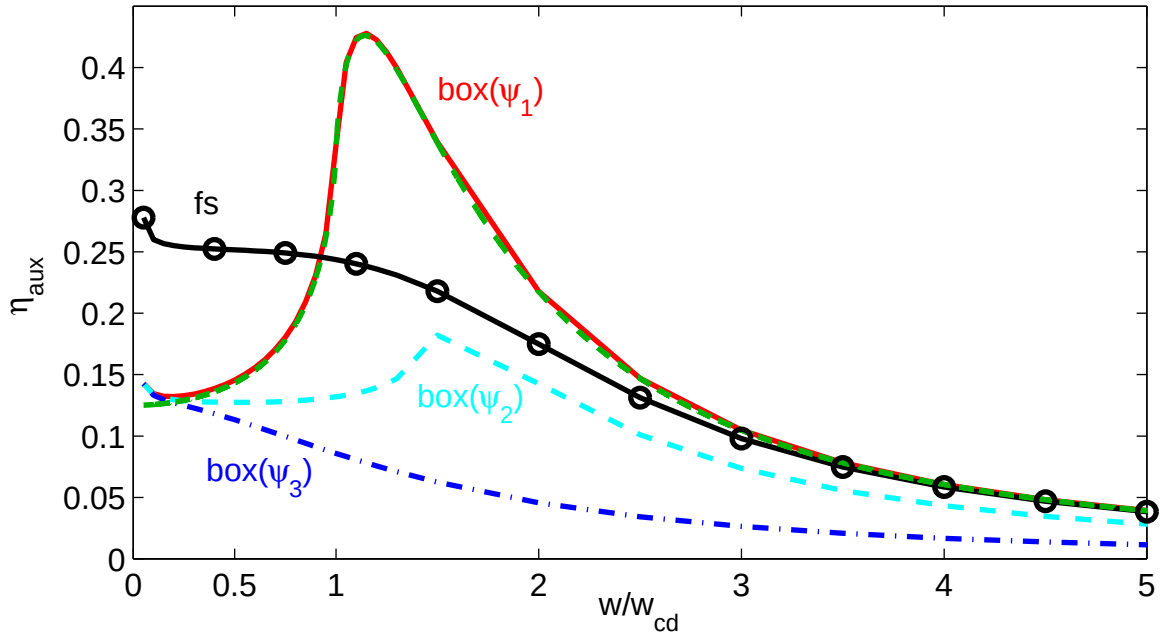

FIG. 2: $\eta_{aux}(w/w_{cd})$, Eq. (16), using the box current density profiles given by Eq.(18) with $\psi_0 = \psi_1$, ψ_2 and ψ_3, and using Eq.(19) (fs). The dashed line on top of the solid line for the box(ψ_1) case corresponds to the analytical result of Ref. 5 (Eq.(17) divided by $(w/w_{cd})^2$).

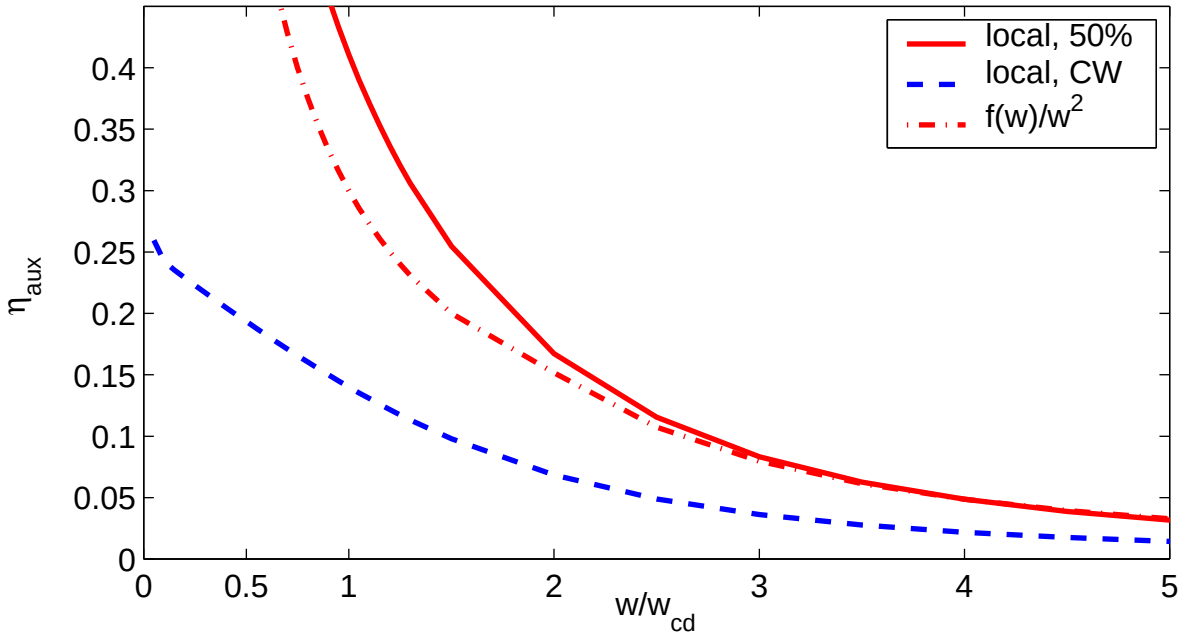

FIG. 3: $\eta_{aux}(w/w_{cd})$, Eq. (9), using the current density defined in Eq.(21) for the 50% on-time (solid line) and CW cases (dashed line). The fit proposed in Ref. 21, Eq. (5), is also shown (dashed-dotted line).

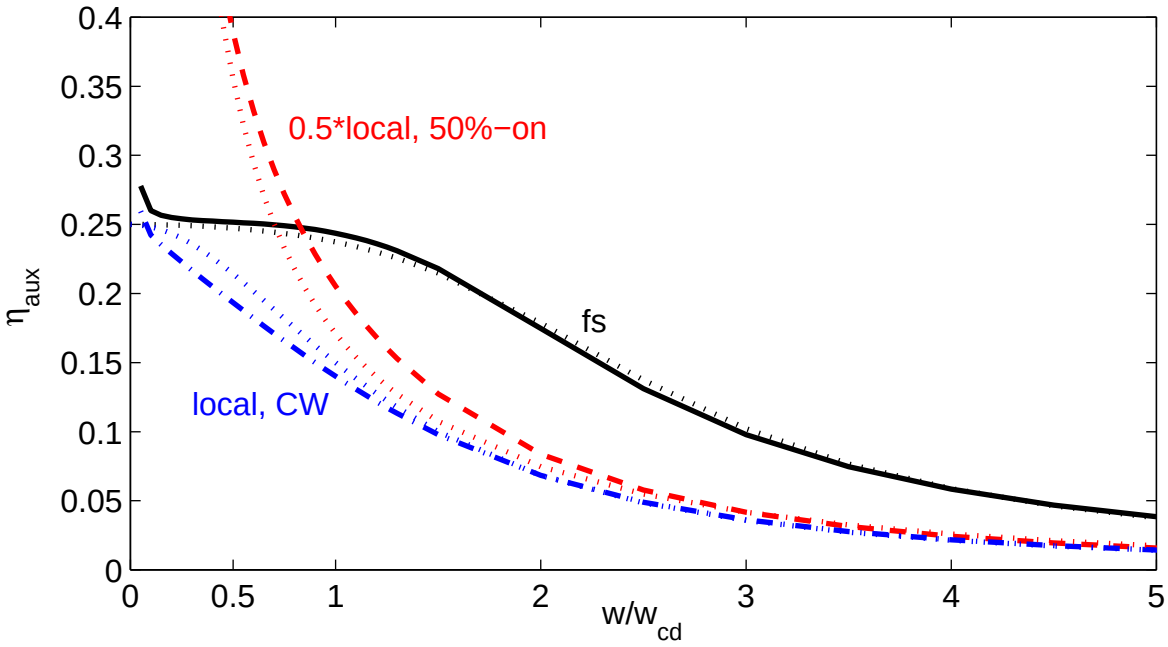

FIG. 4: Comparison of the main results shown in Fig. 2 (fs) and Fig.3 (50% and CW), including the effective total driven current factor I_{cd}/I_{cdCW}. The dotted lines correspond to the analytical fits proposed in Eqs.(20), (22) and (23), respectively.

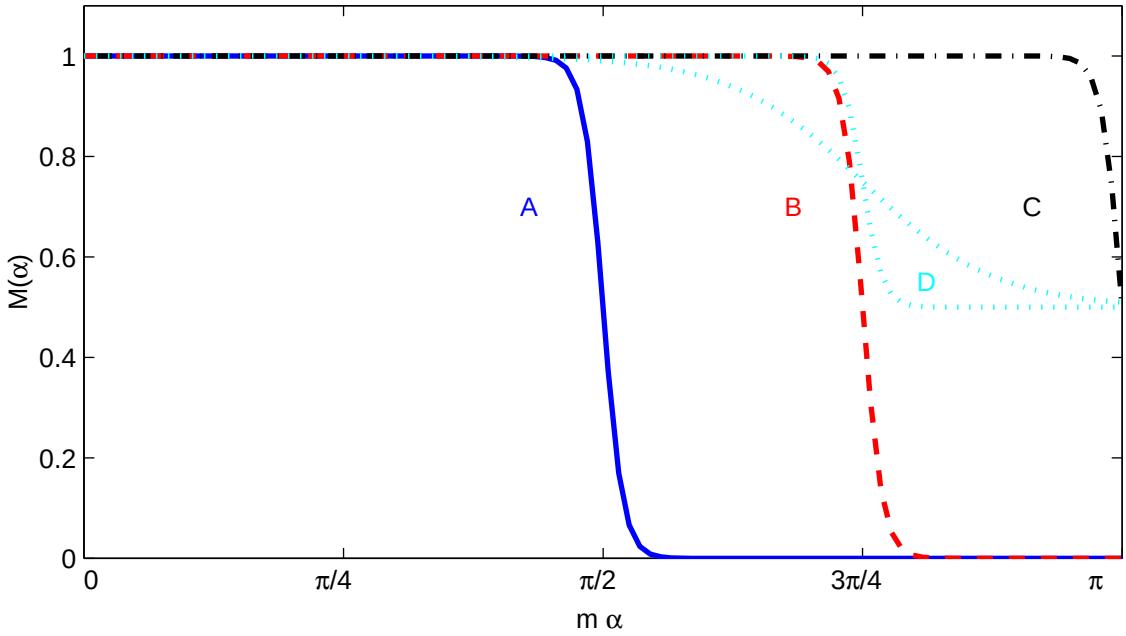

FIG. 5: Various $M(\alpha)$ functions tested to calculate η_{aux} using Eq.(21). The profiles A and C reproduce the results shown in Fig. 3, 50%-on and CW respectively. The profiles D yield similar functions $\eta_{aux}(w/w_{cd})$ as shown in Fig. 7 (solid lines with circles).

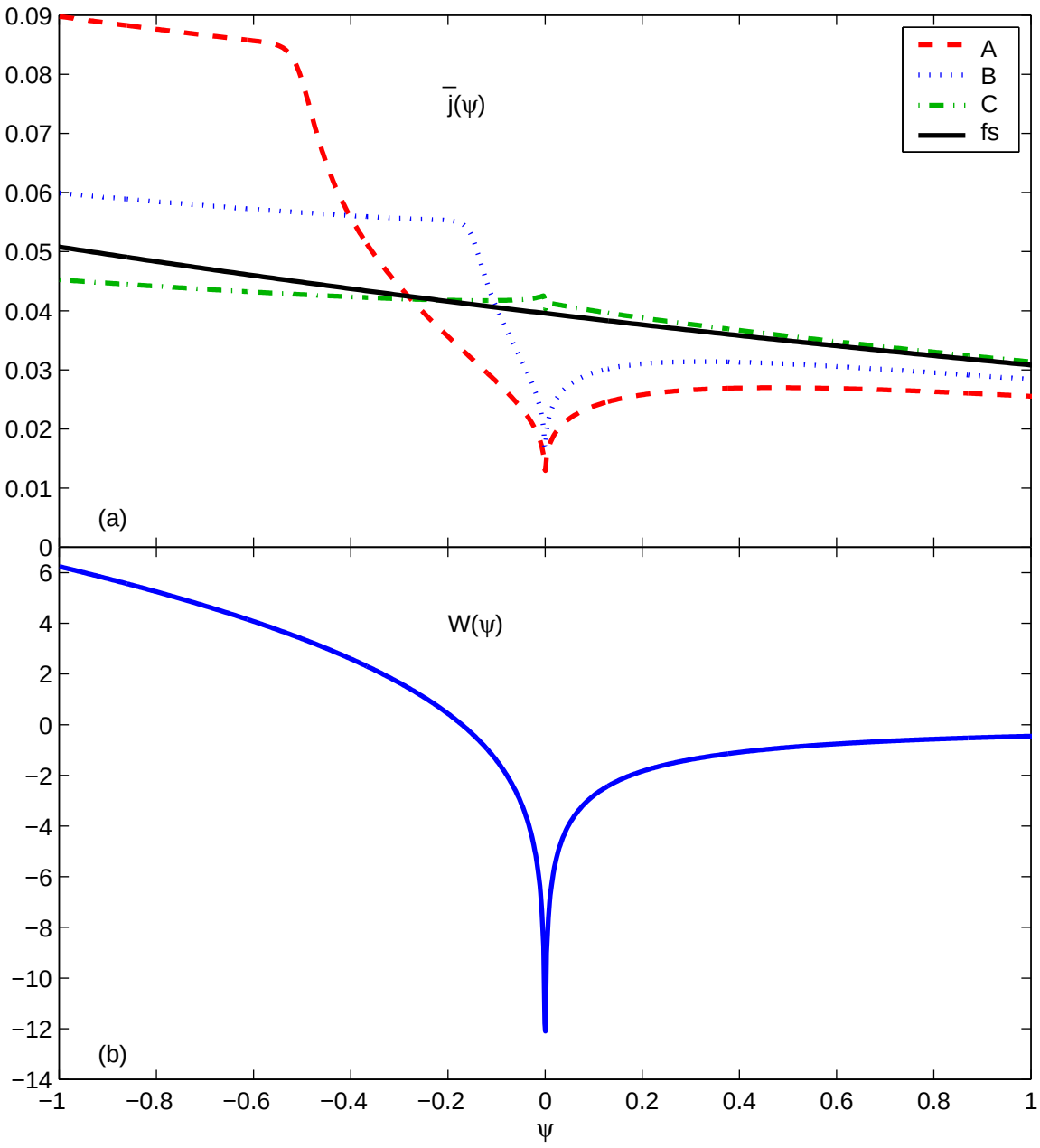

FIG. 6: (a) Flux surface averaged current density profile for $w/w_{cd} = 0.5$, Eq.(24), for the cases A, B and C of Fig. 5, using Eq.(21), and for the fs profile, Eq.(19). (b) Weight function $W(\psi)$ given by Eq.(11).

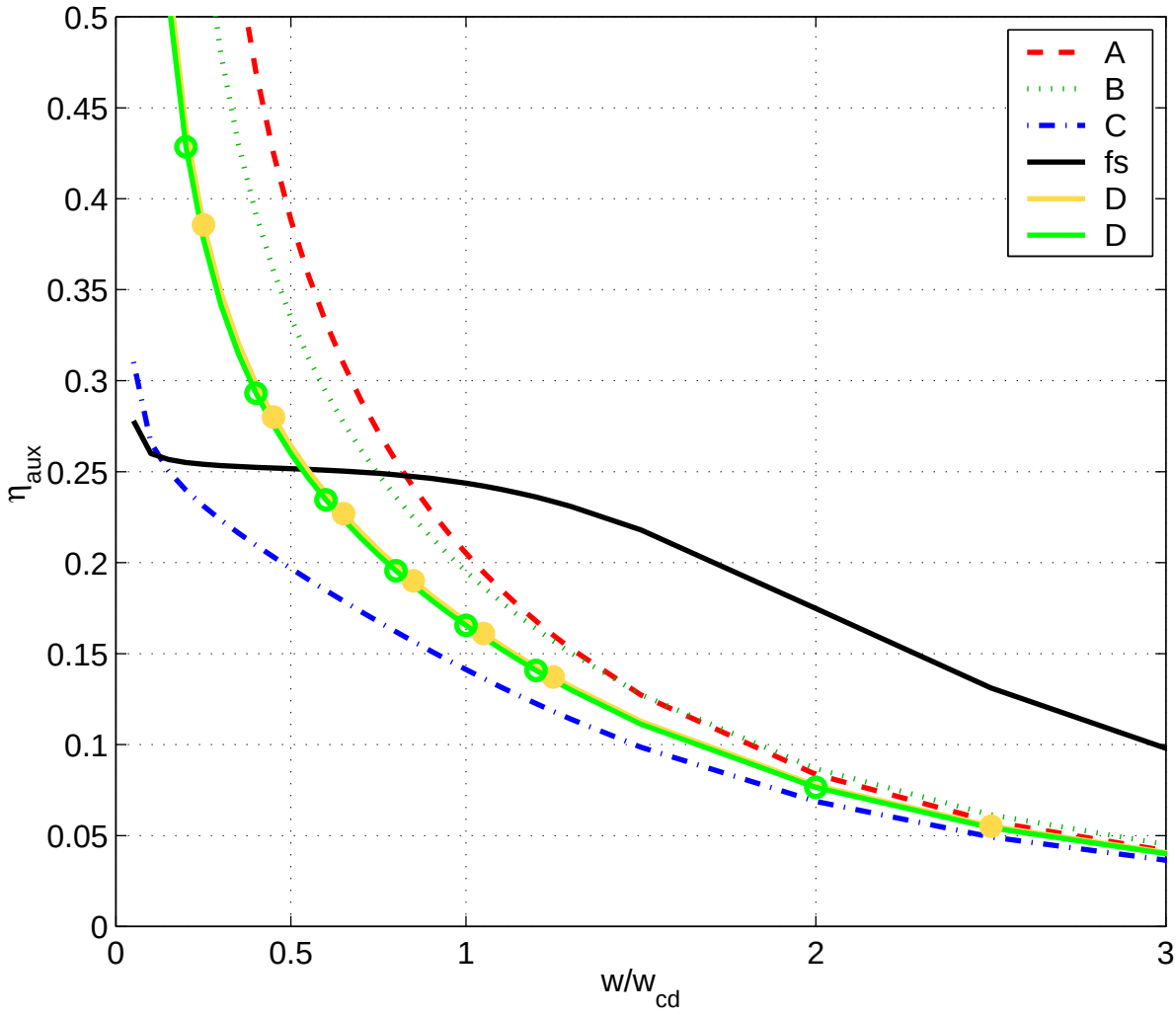

FIG. 7: $\eta_{aux}(w/w_{cd})$ for the current density profiles shown in Fig.(6a), including a factor 0.5, 0.75 for A and B, and 0.87 for the solid line with circles (D cases of Fig. 5), accounting for the effective total driven current.